Numerical and Experimental Study on Spout Elevation in Spout-Fluidized Beds

M.S. van Buijtenen
Dept. of Chemical Engineering and Chemistry, Eindhoven University of Technology, 5600 MB Eindhoven, The Netherlands

K. Buist
Faculty of Science and Technology, Institute for Mechanics Processes and Control Twente, University of Twente, Enschede, 7500 AE, The Netherlands

N.G. Deen, and J.A.M. Kuipers
Dept. of Chemical Engineering and Chemistry, Eindhoven University of Technology, 5600 MB Eindhoven, The Netherlands

T. Leadbeater, and D.J. Parker
Positron Imaging Centre, School of Physics and Astronomy, University of Birmingham, Birmingham B15 2TT, U.K.

DOI 10.1002/aic.12765
Published online September 21, 2011 in Wiley Online Library (wileyonlinelibrary.com).

The effect of elevating the spout on the dynamics of a spout-fluidized bed, both numerically and experimentally is studied. The experiments were conducted in a pseudo-two-dimensional (2-D) and a cylindrical three dimensional (3-D) spout-fluidized bed, where positron emission particle tracking (PEPT) and particle image velocimetry (PIV) were applied to the pseudo-2-D bed, and PEPT and electrical capacitance tomography (ECT) to the cylindrical 3-D bed. A discrete particle model (DPM) was used to perform full 3-D simulations of the bed dynamics. Several cases were studied, that is, beds with spout heights of 0, 2, and 4 cm. In the pseudo-2-D bed, the spout-fluidization and jet-in-fluidized-bed regime, were considered first, and it was shown that in the spout–fluidization regime, the expected dead zones appear in the annulus near the bottom of the bed as the spout is elevated. However, in the jet-in-fluidized-bed regime, the circulation pattern of the particles is affected, without the development of stagnant zones. The jet-in-fluidized-bed regime was further investigated, and additionally the experimental results obtained with PIV and PEPT were compared with the DPM simulation results. The experimental results obtained with PIV and PEPT agreed mutually very well, and in addition agreed well wtih the DPM results, although the velocities in the annulus region were slightly over predicted. The latter is probably due to the particle-wall effects that are more dominant in pseudo-2-D systems compared with 3-D systems. In the jet-in-fluidized-bed regime, the background gas velocity is relatively high, producing bubbles in the annulus that interact with the spout channel. In the case of a non elevated spout, this interaction occurs near the bottom of the bed. As the spout is elevated, this interaction is shifted upwards in the bed, which allows the bubbles to remain undisturbed providing the motion of the particles in the annulus near the bottom of the bed. As a result, no dead zones are created and additionally, circulation patterns are vertically stretched. These findings were also obtained for the cylindrical 3-D bed; although, the effects were less pronounced. In the cylindrical 3-D bed the PEPT results show that the effect on the bed dynamics starts at $h_{spout} = 4$ *cm, which is confirmed by the ECT results. Additionally, ECT measurements were conducted for* $h_{spout} = 6$ *cm to verify if indeed the effect happens at larger spout heights. The root mean square of the particle volume fraction slightly increased at* $h_{spout} = 2$ *cm, whereas a larger increase is found at* h_{spout} *4 and 6 cm, showing that indeed more bubbles are formed. The presented results have not been reported so far and form valuable input information for improving industrial granulators.* © 2011 American Institute of Chemical Engineers *AIChE J,* 58: 2524–2535, 2012
Keywords: spout-fluidized beds, granulation, elevated spout, spout (nozzle), height, particle image velocimetry, discrete particle model

Introduction

Spout-fluidized beds combine the favorable properties of both spouted and fluidized beds and are frequently used for the production of granules or particles through granulation, which is widely applied, for example, in the production of

Correspondence concerning this article should be addressed to N. G. Deen at N.G.Deen@tue.nl.

detergents, pharmaceuticals, food, and fertilizers. Spout-fluidized beds have a number of advantageous properties, such as high mobility of the particles preventing undesired agglomeration and enabling excellent heat transfer control.[1] As typically large (type Geldart D) particles are involved and a relatively small spout nozzle, the ratio between the inlet nozzle and particle diameter is quite small by which the spout channel is formed by the ratio of spout gas and background fluidization velocity.[2,3] This feature provides good mixing and thus highly influences the performance of the granulator. In industry, the spout is slightly elevated from the bottom of the bed to enable efficient spraying of liquid. However, research has so far mainly been focused on non elevated spouts. Related research has been done on spouted beds with draft or Wurster tubes, showing that the degree of mixing is influenced by the dimensions and position of the draft tube.[4–6] In these types of beds, the effect of the spout channel is physically imposed by a draft tube, whereas in spout-fluidized beds, the spout channel arises from the ratio of the spout gas and background fluidization gas velocity. Although it has been demonstrated that draft tubes highly influence the circulation patterns inside spouted beds, the effect of an elevated spout in spout-fluidized beds is not known, and is therefore, the topic of this work. Both experiments and simulations were conducted. The experiments were carried out on a pseudo-two dimensional (2-D) and a cylindrical three dimensional (3-D) bed, where positron emission particle tracking (PEPT) and particle image velocimetry (PIV) were applied to the pseudo-2-D bed, and PEPT and electrical capacitance tomography (ECT) to the cylindrical 3-D bed. The simulations were conducted with a full 3-D discrete particle model (DPM), originally developed by Hoomans et al.[7] and further developed by Link et al.[8] With PIV, the particle flow field in a pseudo 2-D spout-fluidized bed can be obtained. Several workers applied PIV to study 2-D granular flows, such as gas-fluidized beds.[9,10] spout-fluidized beds,[11] spouted beds,[12] but also vibrated granular beds,[13,14] rotating drums,[15] and silos or hoppers.[16,17] Through these applications, PIV has become a powerful tool for flow field measurements in granular media.

PEPT finds its origin in the commonly used medical diagnostic technique of positron emission tomography PET and was developed at the University of Birmingham. A single active particle is tracked, making it a non intrusive measurement technique with the additional advantage that it can be applied to 3-D systems which are not optically accessible. As a single particle is tracked, the disadvantage is, however, that long measurement times are necessary to obtain statistically reliable results. Nevertheless, PEPT has proven to be a rather precise technique, and several workers have used it for various applications. Seville et al.[18] summarized examples of such applications in several types of solids processing equipment Top spray fluidization was investigated by Depypere et al.[19] and circulating fluidized beds were studied using PEPT by Chian et al.[20] and van Velden et al.[21] PEPT was applied to fluidized beds,[22–25] where Laverman et al. were the first who compared experimental PIV results with PEPT.[25] Link et al. used PEPT to study spout-fluidized beds and compared their results with DPM simulations.[26] In this work, PEPT is applied to a pseudo-2-D and a cylindrical 3-D bed, where for the pseudo-2-D bed, the PEPT results will be compared with results obtained with PIV and DPM simulations.

ECT is based on the difference in permittivity of two non conductive materials inside a system, which has been compared with other advanced measurement techniques by Mudde.[27] An image is obtained that represents the particle volume fraction in a 2-D slice of the cross-sectional area of the bed. It is a low cost technique, with high temporal but low spatial resolution. The measurement rate is up to 100 Hz, which makes it suitable for online monitoring and control. However, the image quality depends on the interaction of the probing field and the materials present in the measurement volume (i.e., soft field effects) and on the image reconstruction that is used.[28] As a result, the development and improvement of reconstruction techniques are often topic of research. Isaksen et al.[29] outlines and Yang and Peng[30] assesses various algorithms for the reconstruction, and Li and Yang[31] improved the conventional Landweber algorithm, while Lei et al.[32] improved the Tikhonov algorithm. Several workers applied ECT to study gas–solid flows, such as circulating fluidized beds[33,34] and fluidized beds.[35–37] In this work, ECT is applied to a cylindrical 3-D spout-fluidized bed yielding valuable results (despite its low spatial resolution) in particular in combination with the PEPT technique.

The objective of this work is to both experimentally and numerically study the effect of an elevated spout on the bed dynamics in a pseudo-2-D and cylindrical 3-D spout-fluidized bed. The organization of this article is as follows: first, the numerical model is described. Then, the experimental set-ups and the experimental techniques are explained. Two's, flow-regimes in the pseudo-2-D bed will be studied using PIV, which will be shown first, followed by one-flow regime that is compared with PEPT and DPM results. Finally, the experimental results obtained by PEPT and ECT of the same flow regime in the cylindrical 3-D bed is shown.

Numerical Model

The simulations were conducted with a full 3-D DPM that describes the dynamics of the continuous gas phase and particles. The momentum transfer between the gas phase and particles is accounted for as well as particle–particle and particle–wall collisions, which are described with a soft sphere model. In this approach, the particles are assumed to undergo deformation during their contact, where the contact forces are calculated from a simple mechanical analog involving a spring, a dash-pot, and a slider. This allows for energy dissipation due to non ideal particle interaction by means of the empirical coefficients of normal and tangential restitution, and the coefficient of friction. In case a particle is in contact with several other particles, the net contact force follows from the addition of all binary contributions. This approach was originally proposed by Cundal and Strack[38] for granular matter. For further details on the collision model, the interested reader is referred to the work of Hoomans et al.[7] and Deen et al.[39] The motion of each individual particle present in the system is calculated from the Newtonian equations of motion:

$$m_{\mathrm{p}}\frac{d\mathbf{v}_{\mathrm{p}}}{dt} = -V_{\mathrm{p}}\nabla p + \frac{V_{\mathrm{p}}\beta}{\varepsilon_{\mathrm{p}}}(\mathbf{u}_{\mathrm{f}} - \mathbf{v}_{\mathrm{p}}) + m_{\mathrm{p}}\mathbf{g} + \sum_{N_{\mathrm{p}}}\mathbf{F}_{\mathrm{p}\leftrightarrow\mathrm{p}} + \sum_{N_{\mathrm{w}}}\mathbf{F}_{\mathrm{p}\leftrightarrow\mathrm{w}} \tag{1}$$

$$I_{\mathrm{p}}\frac{d\boldsymbol{\omega}_{\mathrm{p}}}{dt} = \mathbf{T}_{\mathrm{p}} \tag{2}$$

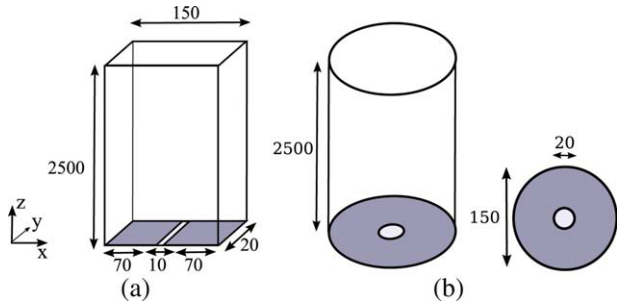

Figure 1. Schematic overview of the experimental pseudo-2-D (a) and cylindrical 3-D (b) spout-fluidized bed, with dimensions in mm.

where the moment of inertia is defined as

$$I_p = \frac{2}{5} m_p r_p^2 \tag{3}$$

and β represents the inter phase momentum transfer coefficient due to drag, which is calculated using a drag relation proposed by Koch and Hill[40] based on lattice-Boltzmann simulations

$$\beta = \frac{18\mu_f \varepsilon_f^2 \varepsilon_p}{d_p^2}\left(F_0(\varepsilon_p) + \frac{1}{2}F_3(\varepsilon_p)\mathrm{Re}_p\right) \tag{4}$$

where $\varepsilon_f + \varepsilon_p = 1$ and Re_p is given by

$$\mathrm{Re}_p = \frac{\varepsilon_f \rho_f |\mathbf{u}_f - \mathbf{v}_p| d_p}{\mu_f} \tag{5}$$

and with

$$F_0(\varepsilon_p) = \begin{cases} \frac{1+3\sqrt{\frac{\varepsilon_p}{2}}+\frac{135}{64}\varepsilon_p \ln(\varepsilon_p)+1614\varepsilon_p}{1+0.681\varepsilon_p-8.48\varepsilon_p^2+8.16\varepsilon_p^3} & \text{if } \varepsilon_p < 0.4 \\ \frac{10\varepsilon_p}{\varepsilon_f^3} & \text{if } \varepsilon_p \geq 0.4 \end{cases} \tag{6}$$

$$F_3(\varepsilon_p) = 00673 + 0.212\varepsilon_p + \frac{0.0232}{\varepsilon_f^5} \tag{7}$$

The gas phase flow field is computed from the volume-averaged Navier–Stokes equations given by:

$$\frac{\partial}{\partial t}(\varepsilon_f \rho_f) + \nabla \cdot (\varepsilon_f \rho_f \mathbf{u}_f) = 0 \tag{8}$$

$$\frac{\partial}{\partial t}(\varepsilon_f \rho_f \mathbf{u}_f) + \nabla \cdot (\varepsilon_f \rho_f \mathbf{u}_f \mathbf{u}_f) = -\varepsilon_f \nabla p - \nabla \cdot (\varepsilon_f \tau_f) - \mathbf{S}_p + \varepsilon_f \rho_f \mathbf{g} \tag{9}$$

where the fluid density, ρ_f, is determined using the ideal gas law and the viscous stress tensor, τ_f is assumed to obey the general form for a Newtonian fluid[41]

$$\tau_f = -\left[\left(\lambda_f - \frac{2}{3}\mu_f\right)(\nabla \cdot \mathbf{u}_f)\mathbf{I} + \mu_f\left((\nabla \mathbf{u}_f) + (\nabla \mathbf{u}_f)^{\mathbf{T}}\right)\right] \tag{10}$$

Two-way coupling is achieved via the sink term, $\mathbf{S}_p$, which is computed from

$$\mathbf{S}_p = \frac{1}{V_{\mathrm{cell}}} \sum_{\forall i \in \mathrm{cell}} \frac{V_i \beta}{\varepsilon_p}(\mathbf{u}_f - \mathbf{v}_i) D(\mathbf{r} - \mathbf{r}_i) \tag{11}$$

The distribution function, D, distributes the reaction force acting on the gas phase to the velocity nodes in the staggered Eulerian grid.

Experimental Set-Up

The pseudo 2-D and cylindrical 3-D bed used in this work are schematically presented in Figure 1. Background fluidization air was supplied by a two-stage side channel blower, having a maximum capacity of 312 m^3/h, a maximum supply pressure of 580 mbar, and a power of 7.5 kW. To prevent electrostatic charging of the particles, the background fluidization air was humidified till ~50% relative humidity with the aid of a spray tower. The spout air was supplied by a second two-stage side channel blower, with a maximum capacity of 205 m^3/h, a maximum supply pressure of 500 mbar, and a power of 4.0 kW. The flow rates of both background and spout sections were controlled by two frequency controllers and were measured by two turbine flowmeters.

The depth of the pseudo-2-D bed was assumed to be sufficiently small to display pseudo-2-D behavior and large enough to avoid extreme particle–wall interaction. The front and back walls of the bed consisted of a Lexan plate to enable visual detection of the particle motion, and the side walls of the bed were made of aluminium strips. The fluidization section was covered with a 3-mm-thick porous plate with an average pore size of 100 μm and the spout section was covered with a 2.0 mm gauze.

The column of the cylindrical 3-D bed consisted of a PVC tube, whereas the bottom section was made of either metal for the PEPT measurements or plastic for the ECT measurements. The latter is done to avoid problems with the ECT measurements. The distributor plate of the fluidization section contained 1.0 mm holes to limit the pressure drop. However, due to this low-pressure drop the distribution of the background fluidization air was slightly non uniform. The spout tube was covered with a 2.0 mm gauze for the metal section, and in the ECT measurements the plastic spout tube was covered with the same distributor plate as the plastic fluidization section.

For the PIV measurements on the pseudo-2-D bed, digital images were recorded with a high speed camera (LaVision Imager Pro) equipped with a 50 mm lens. The aperture of the camera was set to f6 and the exposure time was fixed at 0.4 ms. The recorded images consisted of 608 × 1280 pixels and were stored in the memory of the camera. After all the images for one experiment were recorded, the 12-bit images were transferred to the hard disk of the PC. As shown in Figure 2, the pseudo-2-D bed was illuminated by two 500 W halogen lamps that were positioned in such a way that the bed was illuminated under a small angle (<45°), preventing undesired reflections. The lamps were fed by a direct current supply to minimize temporal variation in the illumination. The back wall was painted black to provide better contrast between particles and gas.

To carry out PEPT measurements, the spout-fluidized bed (either pseudo-2-D or cylindrical 3-D) was positioned in between the two PEPT detectors, as shown in Figure 3. The detectors covered a measurement height of 0.50 m and a width of 0.40 m.

In Figure 4, a schematic illustration of the ECT set-up is presented. The ECT measurements were conducted in a cylindrical 3-D bed, for which a special column was prepared

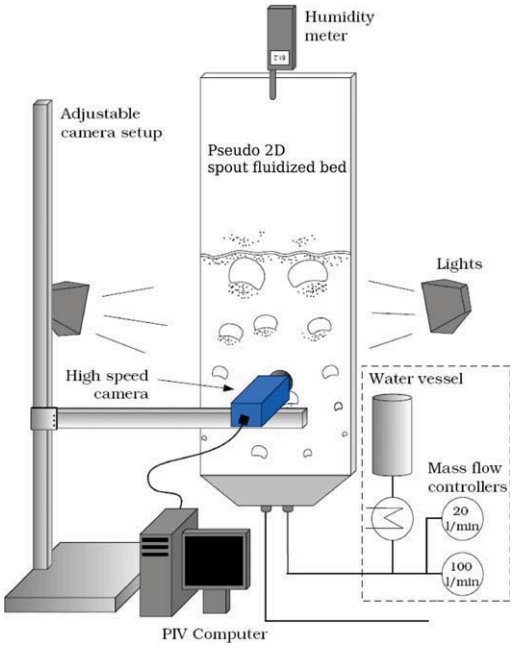

Figure 2. Experimental set-up of PIV measurement technique for pseudo-2-D spout-fluidized bed.

[Color figure can be viewed in the online issue, which is available at wileyonlinelibrary.com.]

containing the ECT sensor that was mounted around the column circumference. An earthed screen was mounted around the sensor and shielded cables were used to connect the sensor to the data acquisition unit (Figure 4). The ECT sensor was self-designed and constructed, whereas commercial ECT computer hardware and software were supplied by Process Tomography. It consisted of two measurement planes, each with 12 measurement electrodes. To prevent the electrical field from being diverted to earth at the ends of the measurement electrodes, guard electrodes surround the measurement electrodes as shown in Figure 5. The first and second measurement planes were located 5 and 15 cm above the bottom plate, respectively. The measurements lasted 5 min, using a frequency of 100 Hz and a pixel resolution of 32×32 to represent the sensor cross-sectional area, which makes a total of 1024 permittivity values per image (pixel area: 0.18 cm^2). The sensor was calibrated before each measurement and to assure that the capacitances remained constant during a measurement; the capacitance of a static bed were measured before and after each measurement. If the measured volume fraction of the static bed remained constant, no shift in capacitance occurred during the fluidization measurement. The Landweber iteration method was used for the image reconstruction, for which the number of iterations and a relaxation parameter were set to, respectively, 110 and 0.01.

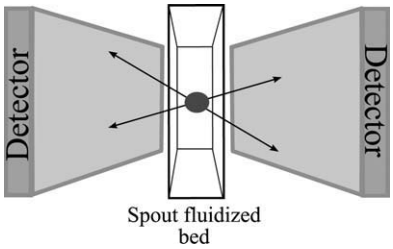

Figure 3. Experimental set-up of PEPT measurement technique including the radio-actively labeled particle emitting back-to-back γ-rays (represented by $\leftrightarrow$).

Note that the pseudo-2-D bed is presented, and that the cylindrical 3-D bed is placed in between the detectors as well.

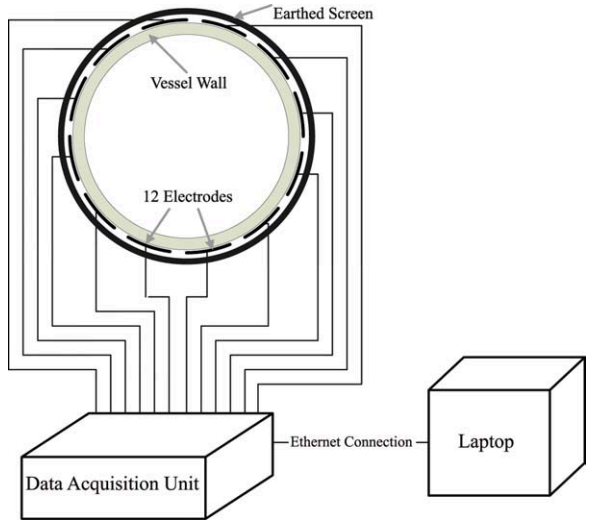

Figure 4. Experimental set-up of ECT measurement on the cylindrical 3-D spout-fluidized bed.

[Color figure can be viewed in the online issue, which is available at wileyonlinelibrary.com.]

Experimental Techniques

Particle image velocimetry

PIV is an optical, nonintrusive measurement technique that produces instantaneous 2-D velocity data for a whole plane in a 3-D flow field. It was originally developed in the field of experimental fluid dynamics to study the flow of single phase fluids.[42] In this work, PIV has been applied to study the particle flow in a pseudo-2-D spout-fluidized bed. The front view of the bed is recorded using the equipment

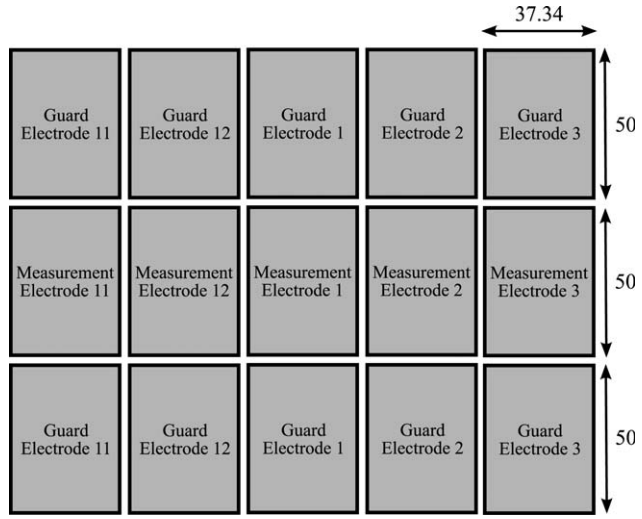

Figure 5. Schematic drawing of five (out of 12) measurement electrodes and guard electrodes for one measurement plane, with dimensions in mm.

shown in Figure 2. Two subsequent images of the flow, separated by a short time delay, Δt, are divided into small interrogation areas. Cross-correlation analysis is used to determine the volume-averaged displacement, $\mathbf{s}_p(\mathbf{x},t)$, of the particle images between the interrogation areas in the first and second image. The velocity within the interrogation area is then easily determined by dividing the measured displacement by image magnification, M, and the time delay

$$\mathbf{v}_p(\mathbf{x},t) = \frac{\mathbf{s}_p(\mathbf{x},t)}{M\Delta t} \tag{12}$$

provided that Δt is sufficiently small. For further details of this technique, the interested reader is referred to the work of Westerweel.[42] A multi-pass correlation algorithm with a final interrogation size of 32 pixel and an overlap of 50% was used to obtain the final velocity field. The particle density in most regions is well above the recommended value of 10,[42] that is, much higher than one would have with conventional PIV that uses seeding particles. We used a standard median filter for postprocessing the vector fields, yielding less than 2% outliers. We used 200 vector fields to compute the time-averaged results, leading to a small random error in the time-averaged velocity fields (i.e., <1%). Unfortunately, the time-averaged PIV data also contain a systematic bias error. This error arises when we calculate the time-averaged flow fields, where we are forced to assume that the number of particles is constant in the interrogation areas (which is not the case in reality). It would be better to weigh the instantaneous velocities with the number of particles that are associated.[43] By comparing the (unweighted) PIV results with those obtained from PEPT, the systematic bias error is estimated to be about 20%.

Positron emission particle tracking

In PEPT, a radioactively labeled particle is detected at high speed by a positron camera. The glass bead (used in this work) is labeled by direct irradiation with a ^{3} He beam, which is generated from a cyclotron, yielding a glass bead that contains the radionuclide $^{1}8$ F with half-life of 110 min. The labeled particle decays with the emission of a positron, and each positron rapidly annihilates with an electron, resulting in an almost exactly back-to-back emisison of a pair of 511 keV γ-rays, which is nonintrusively detected by the two detectors. These detectors define a line of response (LOR) passing close to the active particle. The intersection of several LORs determines the location of the particle in 3-D. In Figure 3, only two LORs are shown.

The position of the tracer particle was recorded over a period of 1.5 h for the pseudo-2-D and 3 h for the cylindrical 3-D bed at a frequency ranging from 100 to 300 Hz depending on the amount of radiation emitted by the single tracer particle and the location of the detectors. The instantaneous particle position is subject to a variable amount of noise, as the detectors are less accurate at the borders of the detectors, and in the horizontal plane, the point of intersection is more difficult to determine due to the small differences in the slopes of the LORs. To obtain accurate results near the bottom of the bed, the spout-fluidized bed is placed at 0.10 m from the lowest border of the detectors, and the noise is furthermore suppressed by applying a cubic spline to the PEPT output data.[26] Because of the (limited) dimensions of the PEPT detectors, the tracer particle occasionally moves out of the detectable area, which is accounted for by leaving out the readings just before exit and after return of the particle in the measurement area. The remaining noise on the time-averaged velocities is diminished by calculating the velocity of the six subsequent particle positions and is subsequently assigned to the cell containing the average over six particle locations. The particle velocity is determined with linear regression, where the least squares method is used to minimize the deviation of the fit to the measurement data

$$\mathbf{v}_p(\mathbf{x},t) = \frac{n\sum_{i=1}^{n}(t\mathbf{x}) - \sum_{i=1}^{n} t \sum_{i=1}^{n} \mathbf{x}}{n\sum_{i=1}^{n}\mathbf{x}^2 - \left(\sum_{i=1}^{n}\mathbf{x}\right)^2} \tag{13}$$

Typical errors in instantaneous PEPT velocity measurement samples are about 10%. For each time-averaged velocity O (100) velocity samples are used, yielding an random error in the time averaged velocities of O (1%).

Electrical capacitance tomography

ECT is based on the measurement of the permittivity distribution (using several electrodes) of two nonconductive materials (in this work air and glass beads), to determine the particle volume fraction. Each electrode is subsequently charged and the capacitance is measured between each electrode pair. The medium (air or glass beads) in between the electrode pairs influences the value of the capacitance, from which the permittivity and thus the particle distribution is reconstructed. The particle distribution in the sensor cross-sectional area is presented on a 32 $\times$ 32 pixel square grid. The sensor is calibrated by measuring the capacitances of an empty bed (lower permittivity material) and of a bed filled with particles (higher permittivity material). Additionally, these values are used to normalize the measured capacitances. The capacitance measurement between the electrode pairs depends on the electrical field lines that appear when one electrode is charged. Because of the varying distances of one electrode to the others, different field lines are present, which result in different capacitance values. This means that the detection of an object depends on its location, that is, the capacitance measured of an object in the center of the bed is different compared with the capacitance of an object near the wall. To account for this variation, the sensitivity at every (pixel) location in the cross-sectional area is determined for each electrode pair and stored in a sensitivity matrix. The sensitivity matrix and the measured capacitance values determine the permittivity at every (pixel) location in the cross-sectional area

$$C_n = S \cdot K \tag{14}$$

C_n is a vector containing 66 measured interelectrode-pair capacitances, K is a vector with permittivity values at the 1024 pixels and S is the sensitivity matrix with dimensions of 66 $\times$ 1024. The permittivity distribution K can be obtained from:

$$K = S^{-1} \cdot C_n \tag{15}$$

where S^{-1} is the inverse of matrix S. However, as S is a nonsquare matrix its inverse matrix does not exist, which is the mathematical consequence of trying to obtain permittivity values for 1024 pixels from 66 capacitance measurements. Because of the limited number of electrode-pair capacitance measurements, insufficient information is available to accurately calculate the permittitivity at every pixel location.

Table 1. Particle Properties

Property	Value	Unit
Material	Glass	–
d_p	3.0	mm
ρ_p	2505	kg/m ^{3}
$e_{n,p\leftrightarrow p}$	0.97	–
$e_{n,p\leftrightarrow w}$	0.97	–
$e_{t,p\leftrightarrow p}$	0.33	–
$e_{t,p\leftrightarrow w}$	0.33	–
$\mu_{p\leftrightarrow p}$	0.10	–
$\mu_{p\leftrightarrow w}$	0.30	–
u_{mf}	1.90*;176†	m/s

* = in pseudo-2D bed.
† = in cylindrical 3D bed.

Therefore, the best possible approximate solution to the problem (i.e., S^{-1}) should be found. This so-called inverse problem can be solved with different reconstruction techniques, such as the linear back-projection (LBP), iterative LBP, Tikhonov regularization, and the Landweber iteration method, as described by Yang and Peng.[30] In this work, the Landweber iteration method is used. The particle volume fraction is calculated using the inverted Maxwell concentration model[37]

$$\varepsilon_p = \frac{2K_{EN}\cdot K_{perm} + K_{EN}}{3K_{perm} + K_{EN} - K_{EN}\cdot K_{perm}} \tag{16}$$

with $K_{perm} = \frac{K_H}{K_L}$ as the permittivity ratio, where K_L is the permittivity of air, whereas K_H is the permittivity of the bed filled with particles, defined as

$$K_H = \varepsilon_{packed} = \varepsilon_{glass}\cdot\alpha + \varepsilon_{air}\cdot(1-\alpha) \tag{17}$$

where ε_{glass} is the relative permittivity of glass, ε_{air} the relative permittivity of air and α the volume fraction of a packed bed ($\approx$0.6). Equation 17 shows that the high permittivity value is a mixture of particles and air, and thus depends on the packing fraction.

K_{EN} is the normalized permittivity value, given by

$$K_{EN} = \frac{K_H\cdot\varepsilon_p + K_L(1-\varepsilon_p) - K_L}{K_H - K_L} \tag{18}$$

The number of iterations and the relaxation parameter for the Landweber reconstruction technique are chosen by finding the smallest capacitance residual[30]

$$C_{res} = \frac{C_n - K_{recon}\cdot S}{C_n}\times 100\% \tag{19}$$

where C_{res} is the capacitance residual, C_n the normalized measured capacitance, S the sensitivity matrix and K_{recon} is the reconstructed permittivity. $K_{recon}\cdot S$ is the capacitance that appears from the reconstructed permittivity and sensitivity matrix, and the capacitance residual is thus a measure for the performance of the reconstruction. By minimizing this value, the optimal reconstruction is obtained. It should be kept in mind that the resulting particle volume fraction satisfies $0 \leq \varepsilon_p \leq 0.6$. Therefore, the choice of the number of iterations and the relaxation parameter is a compromise of achieving the lowest capacitance residual and obtaining realistic values of ε_p.

Table 2. Gas Velocities

System	Flow Regime	u_{bg} (m/s)	u_{sp} (m/s)
Pseudo-2-D	Spout-fluidization†	2.20	43.40 ± 0.50
	Jet-in-fluidized-bed*	4.15 ± 0.15	37.25 ± 0.25
Cylindrical	Jet-in-fluidized-bed**	3.80 ± 0.10	67.15 ± 1.5
3-D	Jet-in-fluidized-bed***	3.60	48.80 ± 0.4

† = PIV.
* = PIV & PEPT & DEM.
** = PEPT.
*** = ECT.

Test Cases

In this work, three spout heights were used, that is 0, 2 and 4 cm above the bottom plate. Additionally, for the cylindrical 3-D bed, a spout height of 6 cm was studied as well as using ECT. The static bed height was kept constant at 10 cm above the spout by increasing the amount of particles, as the spout height increases. In this way, the spout air faces similar resistance to break through the bed for each spout height. The spout gas velocity for ECT measurements in the cylindrical 3-D bed could not be set equal to the spout gas velocity used for the PEPT measurements, due to pressure drop limitations for the plastic bottom section. Nevertheless, the bed dynamics still displayed characteristics of the jet-in-fluidized bed regime, enabling comparison with the PEPT measurements. For details of the flow regimes in a similar 3-D and pseudo-2-D spout-fluidized bed, the reader is referred to the work of Link et al.[44,45] The minimum fluidization velocity was determined experimentally for both the pseudo-2-D and the cylindrical 3-D bed. It appears that the value in the pseudo-2-D bed is higher than in the cylindrical 3-D bed, which is most probable due to the more pronounced particle–wall effect in pseudo-2-D systems. In Tables 1–3, the particle properties, applied gas velocities, and the settings for the numerical simulations are listed.

Results and Discussion

Pseudo-2-D bed: jet-in-fluidized-bed and spout-fluidization regime

PIV measurements were conducted for the jet-in-fluidized-bed and spout-fluidization regime, the results of which are shown in Figure 6. For the spout-fluidization regime, elevation of the spout leads to dead zones in the annulus, but for the jet-in-fluidized bed regime particles in the annulus still move and the vortices are vertically more stretched. In the spout-fluidization regime, the spout gas provides motion of particles by dragging the particles into the spout channel, supported by the background gas. However, in case of an elevated spout, the spout gas influences the particles near the bottom of the bed to a lesser extent and the background velocity is not large enough to compensate for that, causing dead zones in the annulus region. In the jet-in-fluidized bed regime, the background velocity supplies enough air to move the particles in the annulus as the spout height is increased, leading to unexpected particle behavior. Therefore, this regime is further investigated.

Table 3. Numerical Settings for Pseudo-2-D Spout Fluidized Bed Simulation

Property	Value	Unit
N_x	29	–
N_y	2	–
N_z	250	–
Δt	10^{-4}	s
t_{end}	20	s
N_p	$1.2\cdot10^4$; $1.4\cdot10^4$; $1.7\cdot10^4$	–
k_n	10^4	N/m

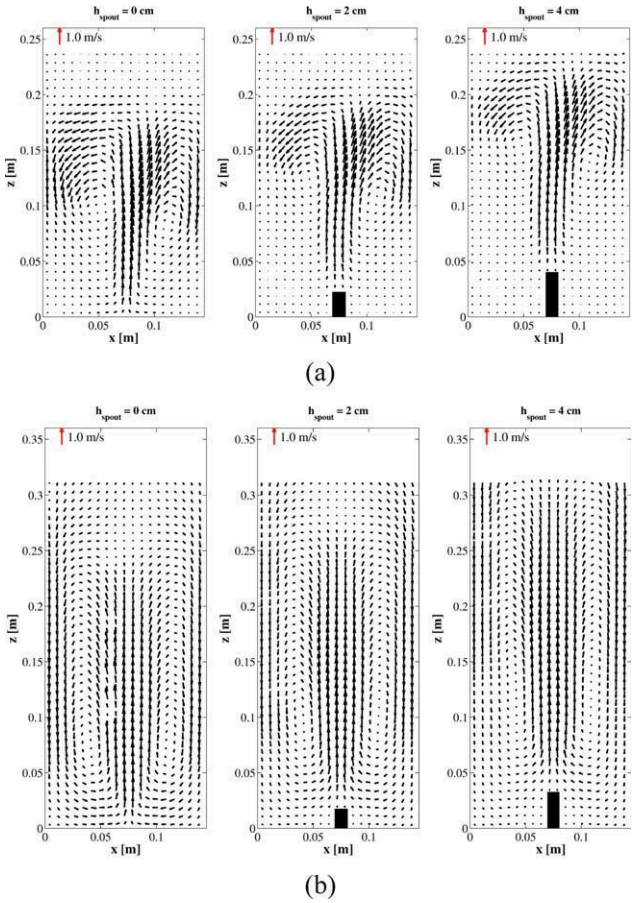

Figure 6. Time-averaged particle velocity fields in the pseudo-2-D bed for h_{spout} = 0 cm (left), h_{spout} = 2 cm (center), and h_{spout} = 4 cm (right) obtained from PIV measurements for the spout-fluidization regime (u_{bg} = 2.2 m/s and u_{sp} = 43.8 m/s) (a) and jet-in-fluidized-bed regime (u_{bg} = 4.0 m/s and u_{sp} = 37.0 m/s) (b).

[Color figure can be viewed in the online issue, which is available at wileyonlinelibrary.com.]

Pseudo-2-D bed: jet-in-fluidized-bed regime

Besides PIV measurements, also PEPT measurements and DPM simulations have been conducted for the pseudo-2-D spout-fluidized bed for the jet-in-fluidized-bed regime. As shown in Figure 7, both experimental techniques and the DPM simulations display the same effect of the spout height.

The velocity profiles in the central xz-plane at $z = 0.10$ m above the spout, as plotted in Figure 8, reveal that the velocity profiles obtained from PIV and PEPT agree very well. Moreover, the DPM simulation results agree well with the experimental data in the spout channel. However, in the annulus region, the DPM slightly overpredicts the downward velocity. In pseudo-2-D beds, the particle–wall effect is more dominant compared with 3-D beds, causing a stronger (but yet small) overprediction in the annulus region. Nevertheless, the overall velocity field is quite well predicted and therefore, the DPM simulations are used to study the bed behavior in more detail.

In Figure 9 the contour plot of the time-averaged horizontal particle velocity obtained from DPM simulations is shown. As the spout height increases, the profiles of the horizontal particle velocity stretch vertically in the bed, whereas the horizontal particle velocity near the bottom boundary slightly decreases. For h_{spout} = 2 cm the velocity profile shifts accordingly, but for h_{spout} = 4 cm, the velocity profile shifts higher up in the bed than the spout elevation. This is most likely due to the bubbles in the annulus region that remain undisturbed near the bottom, as the interaction with the spout occurs at a higher location in the bed. As a result,

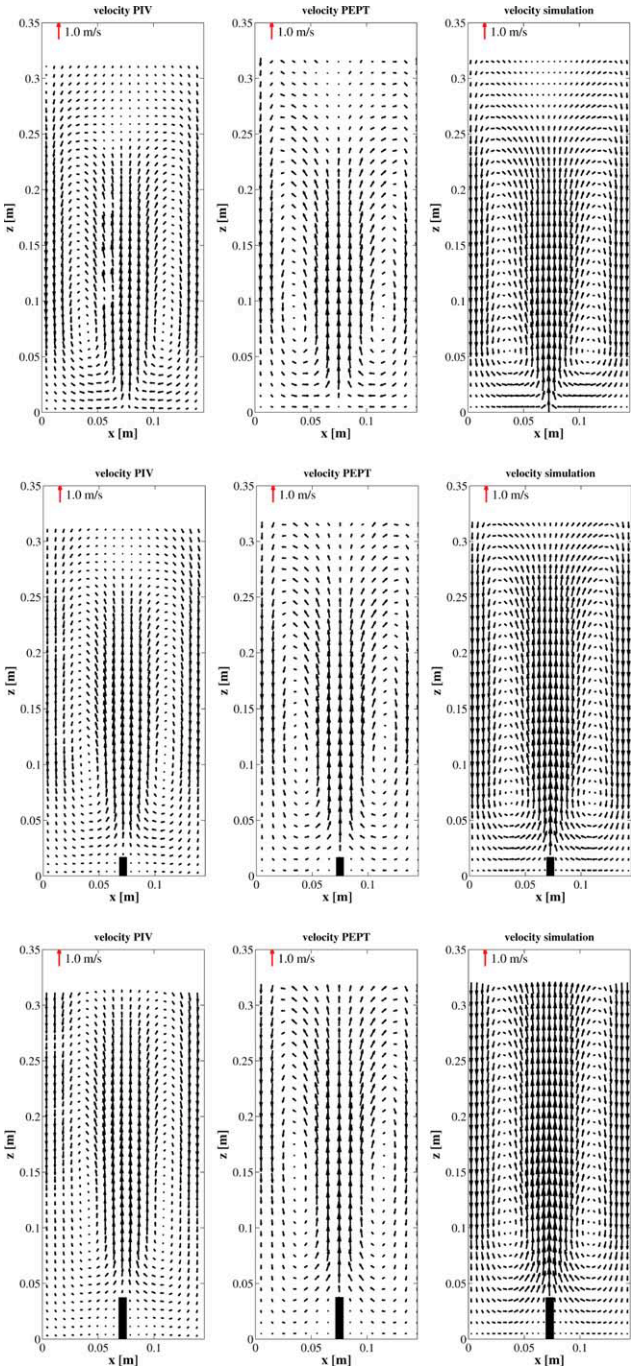

Figure 7. Time-averaged particle velocity fields in the pseudo-2-D bed for jet-in-fluidized-bed regime for h_{spout} = 0 cm (top), h_{spout} = 2 cm (center), and h_{spout} = 4 cm (bottom) obtained from PIV (left), PEPT (center) experiments, and DPM simulations (right).

[Color figure can be viewed in the online issue, which is available at wileyonlinelibrary.com.]

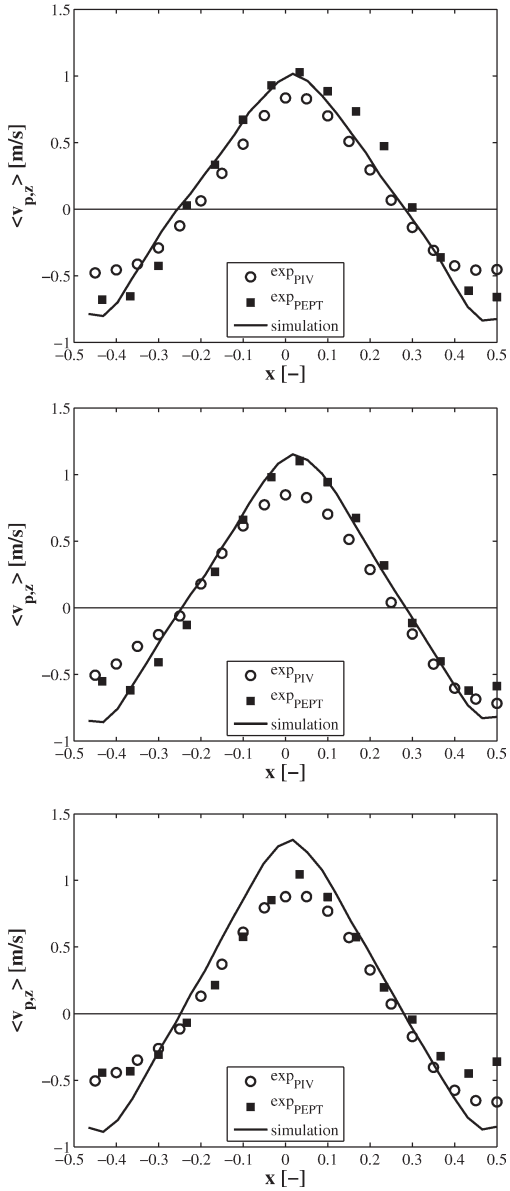

Figure 8. Profiles of the time-averaged vertical particle velocity for the jet-in-fluidized-bed regime in the pseudo-2-D bed obtained from PIV and PEPT measurements and from DPM simulations, in the central *xz*-plane at $z = 0.10$ m above the spout.

This is done to compare the velocity in the same region inside the bed.

the particles in the annulus near the bottom of the bed are still able to move and are dragged higher up in the bed. The bubble formation with increasing spout height is also shown in Figure 10, where the particle volume fraction near the bottom of the bed decreases and the more dense region is located higher up in the bed. Near the spout tube, the particle volume fraction is slightly higher.

Cylindrical 3-D bed: jet-in-fluidized-bed

PEPT and ECT were used to study the cylindrical 3-D spout-fluidized bed. For the PEPT measurements, the particle velocity is determined in axisymmetrical cylinder coordinates. Consequently, the velocity data are mirrored to visualize the full picture in the vector velocity field, as shown in Figure 11.

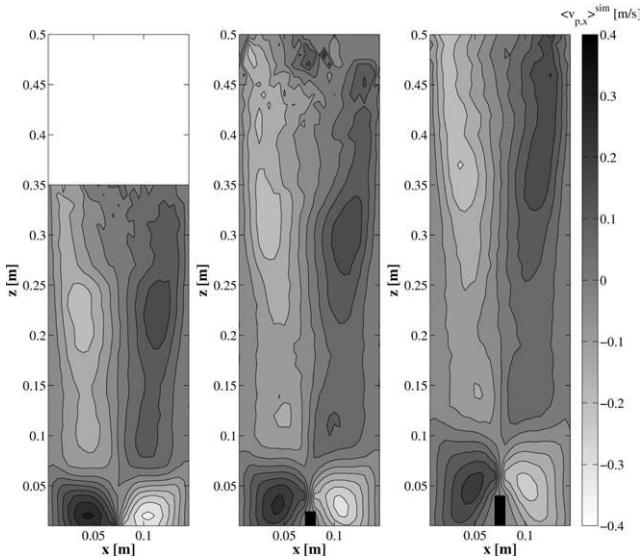

Figure 9. Contour plot of the time-averaged horizontal particle velocity for the jet-in-fluidized-bed regime in the pseudo-2-D bed for $h_{spout} = 0$ cm (left), $h_{spout} = 2$ cm (center), and $h_{spout} = 4$ cm (right), obtained from DPM simulations.

It seems that the effect of spout elevation in the cylindrical 3-D bed is smaller compared with the pseudo-2-D bed, which is due to the less dominant particle–wall effect in 3-D systems. The bubbles in the annulus region are less affected as the spout elevates, causing the vortices in the annulus being less vertically stretched. This is also shown in Figure 12, where the time-averaged radial particle velocity is shown in a contour plot. In this plot, the profiles also stretch vertically as the spout height increases, but to lesser extent

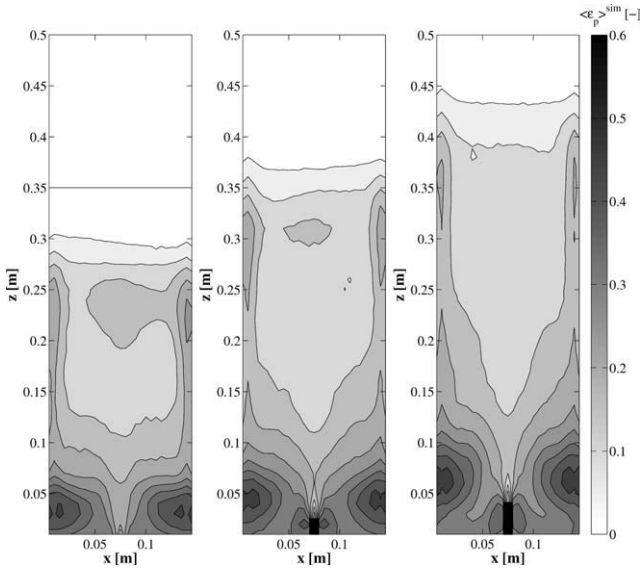

Figure 10. Contour plot of the time-averaged particle volume fraction for the jet-in-fluidized-bed regime in the pseudo-2-D bed for $h_{spout} = 0$ cm (left), $h_{spout} = 2$ cm (center), and $h_{spout} = 4$ cm (right), obtained from DPM simulations.

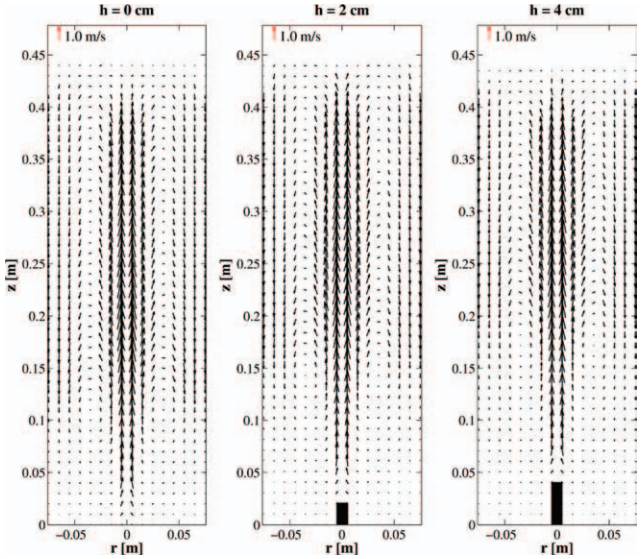

Figure 11. Time-averaged particle velocity field in the cylindrical 3-D bed for h_{spout} = 0 cm (left), h_{spout} = 2 cm (center), and h_{spout} = 4 cm (right) obtained with PEPT measurements for the jet-in-fluidized-bed regime.

Note that only every second vector in each direction is shown for the sake of clarity. [Color figure can be viewed in the online issue, which is available at wileyonlinelibrary.com.]

compared with the pseudo-2-D bed. Both figures display that the particle velocity near the bottom of the bed is much smaller.

As a single particle is tracked in the PEPT technique, the occupancy, that is the time that a particle spends in a grid cell, can be determined using Eq. 20. The time a particle is in the cell depends on the total number of cells that is used. The larger the number of cells, the smaller the occupancy in each cell. Therefore, the occupancy is normalized to the number of cells (N_{cell}). A value of 1 for the occupancy, thus implies that the time a particle spends in each cell is equal.

$$\sigma(\mathbf{x}) = \frac{\sum_{N_t} \Delta t \,\forall\, \mathbf{r}_p \cap \mathbf{x}}{\sum_{N_t} \Delta t} \cdot N_{\text{cell}} \tag{20}$$

As shown in Figure 13, the occupancy near the bottom is quite low implying that the particle does not reach the bottom often, which is in accordance with the low velocity shown in Figures 11 and 12. The area, where the particle is most, is located in the upper region in the annulus, where the particle apparently is dragged into the spout channel and arrives after raining down. This location with the maximum occupancy shifts linearly with the spout elevation. The maximum occupancy at h_{spout} = 4 cm has decreased, which means that the time the particle is in that region had decreased. This could be due to the presence of more bubbles, causing more mixing, and thus more motion of the particles in the annulus region. It seems that at this spout height, the bubbles originating from the background gas still exist and are (just as in pseudo-2-D) affected by the spout gas at a higher location in the bed. Although the bubbles exist longer when the spout is elevated, spout channel is still present indicating that the features of spout-fluidized beds still prevail. Consequently, the effect of spout elevation in the cylindrical 3-D bed starts at h_{spout} = 4 cm instead of 2 cm, and therefore, complementary ECT measurements were conducted at spout heights of h_{spout} = 0, 2, 4, and also 6 cm, to verify if indeed more bubbles are present in the annulus as the spout is elevated further.

The presence of bubbles causes fluctuations in the bed, and hence in the particle volume fraction, which is shown in terms of the root mean square (RMS) in Figure 14. As evident from Figures 14a and b, the RMS of the volume fraction does not change much with a spout elevation from 0 to 2 cm. However, the RMS of the volume fraction at h_{spout} = 4 and 6 cm increases in the annulus region, which is clearly seen in the central profile that is shown in Figure 15. Elevation of the spout at 2 cm does not influence the bubble formation much,

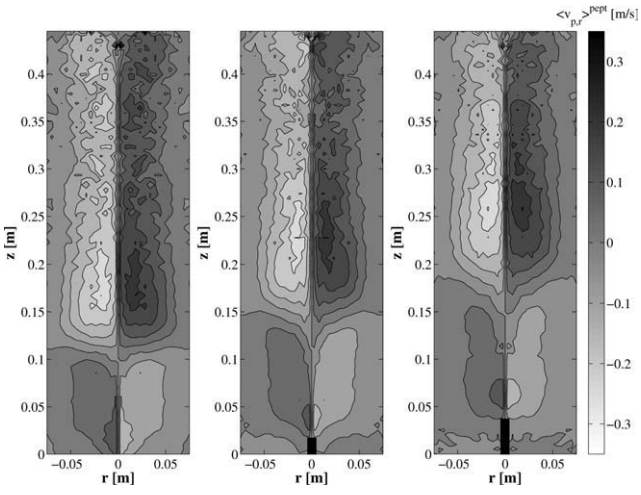

Figure 12. Contour plot of the time-averaged radial particle velocity for the jet-in-fluidized-bed regime in the cylindrical 3-D bed for h_{spout} = 0 cm (left), h_{spout} = 2 cm (center), and h_{spout} = 4 cm (right), obtained with PEPT measurements.

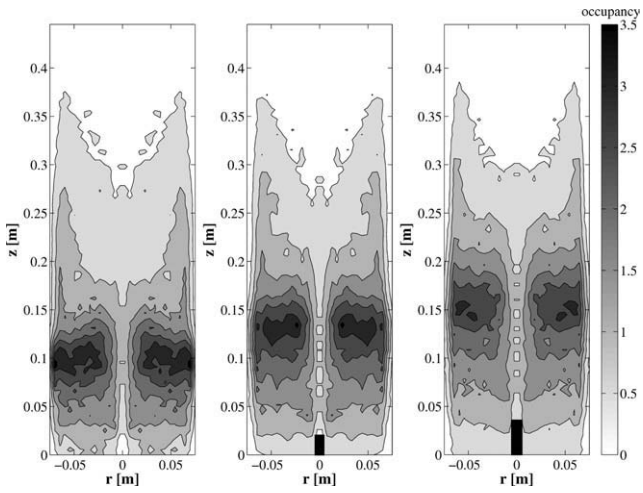

Figure 13. Contour plot of the time-averaged occupancy for the jet-in-fluidized-bed regime in the cylindrical 3-D bed h_{spout} = 0 cm (left), h_{spout} = 2 cm (center), and h_{spout} = 4 cm (right), obtained with PEPT measurements.

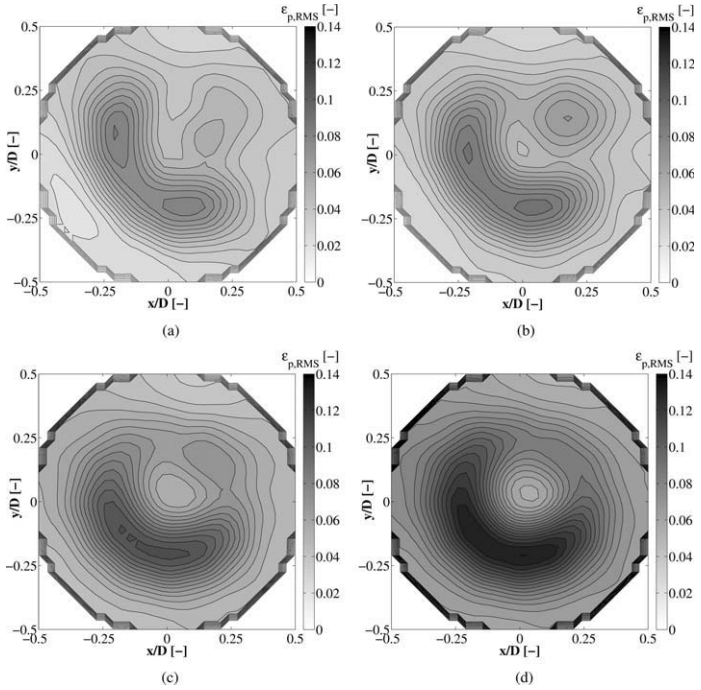

Figure 14. Contour plot of the *xy*-plane of the root mean square (RMS) of the particle volume fraction for h_{spout} = 0 cm with C_{res} = 10.8% (a), h_{spout} = 2 cm with C_{res} = 9.9% (b), h_{spout} = 4 with C_{res} = 10.0% cm (c), and h_{spout} = 6 cm with C_{res} = 10.4% (d), obtained with ECT measurements.

whereas the elevations at 4 and 6 cm clearly have an effect. These ECT results, thus confirm that an elevated spout also influences the dynamics in a cylindrical 3-D bed, which occurs at a higher spout height than in the pseudo-2-D bed.

Conclusions

In this work, the effect of spout elevation on the bed dynamics has been investigated experimentally and computationally using, respectively, noninvasive monitoring techniques and full 3-D Euler–Lagrange simulations. In our study, in both, a pseudo-2-D and a cylindrical 3-D spout-fluidizad bed, with spout heights of 0, 2, and 4 cm has been used. First, two flow regimes have been investigated in the pseudo-2-D bed, from which it was concluded that the spout-fluidization regime did not show any dependency on spout height in the sense that increasing the spout height leads to the creation of dead zones up to the entrance of the spout, yielding a similar situation as a spout-fluidized bed where the spout is not elevated. The jet-in-fluidized-bed regime, however, displayed unexpected particle behavior. Therefore, the jet-in-fluidized-bed regime was investigated further in both the pseudo-2-D and cylindrical 3-D bed.

The experimental techniques PIV and PEPT were applied to the pseudo-2-D bed, showing very good quantitative agreement in the particle velocity implying that both techniques perform correctly. DPM simulations were also conducted, and the results compared quite well with the experimental data. The downward velocity in the annulus region, however, was slightly overpredicted by DPM.

The experimental and simulation results show that due to the elevation of the spout, the bubbles in the annulus remain undisturbed near the bottom of the bed and interact with the spout channel at a higher location depending on the spout height. As a result, the particles still move in the annulus in contrary to the spout-fluidization regime where the particles become stagnant. The high background velocity in the jet-in-fluidized-bed accounts for the enhanced particle motion.

To verify if these phenonema also occur in the cylindrical 3-D spout-fluidized bed, PEPT and ECT measurements were carried out for the jet-in-fluidized-bed regime. The particle velocity profiles obtained by PEPT show that the elevation of the spout influences the bed dynamics to a lesser extent, which was confirmed by the ECT results. ECT measurements were conducted for spout heights up to 6 cm, and it was shown that the effect was observable for $h_{spout} = 4$ and 6 cm. At these spout heights, the fluctuations in the bed (in terms of the RMS of the particle volume fraction)

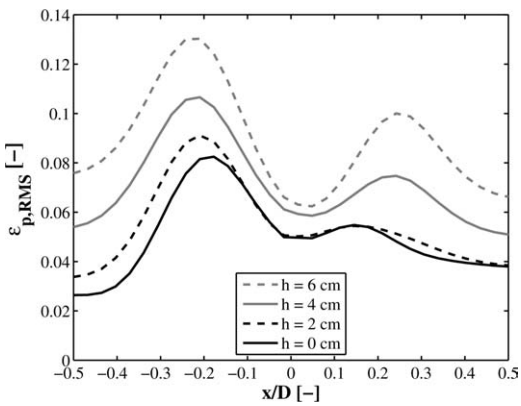

Figure 15. Profile of the root mean square of the particle volume fraction at the central row of the *xy*-plane.

increased obviously, indicating that more bubbles are present in the annulus.

Summarizing, it is showed that the particle behavior near the bottom of the bed is affected differently by the spout elevation for the jet-in-fluidized-bed regime. Instead of creating more dead zones in the annulus region, particles are fluidized by the bubbles. This has not been reported so far, and these findings are of great importance for industry, where the spout is often elevated. This is particularly the case in granulation processes to enable liquid spray through the spout.

Acknowledgments

The authors would like to thank FOM, STW and Yara Sluiskil, The Netherlands, for their financial support to the project. Part of this work is conducted at the University of Twente, Enschede, The Netherlands.

Nomenclature

Roman letters

C = capacitance, F
D = diameter, m
D = distribution function
e_n = coefficient of normal restitution
e_t = coefficient of tangential restitution
$\mathbf{F}_{ab}$ = contact force, N
$\mathbf{g}$ = gravitational acceleration, m/s^2
h_{spout} = spout height, m
$\mathbf{I}$ = unit vector
K = permittivity distribution
k_n = spring stiffness, N/m
M = image magnification
m_p = particle mass, kg
N_{cell} = number of grid cells
N_p = number of particles
N_t = number of timesteps
N_x = number of grid cells x-direction
N_y = number of grid cells y-direction
N_z = number of grid cells z-direction
N_w = number of system walls
n = number of particle locations
p = pressure, Pa
$\mathbf{r}$ = position, m
Re_p = particle Reynolds number
$\mathbf{S}_p$ = particle drag sink term
S = sensitivity matrix
s = volume-averaged displacement vector, m
t = time, s
$\mathbf{T}$ = torque, Nm
Δt = time delay / time step in simulation, s
$\mathbf{u}_f$ = gas velocity, m/s
$\mathbf{v}_p$ = particle velocity, m/s
V = volume, m^3
$\mathbf{x}$ = coordinate vector, m

Greek letters

α = particle volume fraction of packed bed
β = inter-phase momentum transfer coefficient, kg/m^{3}s
ε = volume fraction
ε = relative permittivity
λ_f = gas phase bulk viscosity, kg/ms
μ = dynamic friction coefficient
μ_f = gas phase shear viscosity, kg/ms
ρ = density, kg/m^3
$\mathbf{\Sigma}$ = occupancy
τ_f = gas phase stress tensor, Pa
ω = angular velocity, 1/s

Subscripts

bg = background fluidization
coll = collisions
EN = normalized
end = end of simulation
exp = experimental
f = fluid phase
H = high permittivity material
L = low permittivity material
mf = minimum fluidization
n = normal direction/normalized
p = particle
perm = permittivity ratio
r = radial direction
recon = reconstructed
res = residual
sim = simulation
sp = spout
t = tangential direction
w = wall
x = horizontal direction
z = vertical direction

Abbreviations

2-D = two-dimensional
3-D = three-dimensional
DPM = discrete particle model
ECT = electrical capacitance tomography
LOR = line of response
PEPT = positron emission particle tracking
PIV = particle image velocimetry
RMS = root mean square

Literature Cited

1. Mörl L, Heinrich S, Peglow M. *Granulation (Handbook of Powder Technology)*, Vol. 11. Amsterdam, The Netherlands: Elsevier Science B. V., 2007.
2. Mathur KB, Epstein N. *Spouted Beds*. New York: Academic Press, 1974.
3. Olazar M, San Jose MJ, Aguayo AT, Arandes JM, Bilbao J. Stable operation conditions for gas-solid contact regimes in conical spouted beds. *Ind Eng Chem Res* 1992;31:1784–1792.
4. Chatterjee A. Spout fluid bed technique. *Ind Eng Chem Process Des Dev*. 1970;9:340–341.
5. Kalwar MI, Raghavan GSV, Mujumbar AS. Circulation of particles in two-dimensional spouted beds with draft plates. *Powder Technol*. 1993;77:233–242.
6. da Cunha RLG, Pereira MMC, Rocha SCS. Conventional and modified fluidized bed: comparison of the fluid dynamics and application in particle granulation. *Chem Eng Process* 2009;48:1004–1011.
7. Hoomans BPB, Kuipers JAM, Briels WJ, van Swaaij WPM. Discrete particle simulation of bubble and slug formation in a two-dimensional gas-fluidised bed: a hard-sphere approach. *Chem Eng Sci*. 1996;51:99–118.
8. Link JM, Godlieb W, Deen NG, Kuipers JAM. Discrete element study of granulation in a spout-fluidized bed. *Chem Eng Sci*. 2007;62:195–207.
9. Bokkers GA, Van Sint Annaland M, Kuipers JAM. Mixing and segregation in a bidisperse gas-solid fluidised Bed: a numerical and experimental study. *Powder Technol*. 2004;140:176–186.
10. Dijkhuizen W, Bokkers GA, Deen NG, Van Sint Annaland M, Kuipers JAM. Extension of PIV for measuring granular temperature field in dense fluidized beds. *AIChE J*. 2007;53:108–118.
11. Link JM, Zeilstra C, Deen NG, Kuipers JAM. Validation of a discrete particle model in a 2-D spout-fluid bed using non-intrusive optical measuring techniques. *Can J Chem Eng*. 2004;82:30–36.
12. Liu GQ, Li SQ, Zhao XL, Yao Q. Experimental studies of particle flow dynamics in a two-dimensional spouted bed. *Chem Eng Sci*. 2008;63:1131–1141.
13. Zeilstra C, Collignon JG, Van der Hoef MA, Deen NG, Kuipers JAM. Experimental and numerical study of wall-induced granular convection. *Powder Technol*. 2008;184:166–176.
14. Deng R, Wang CH. Particle image velocimetry study on the pattern formation in a vertically vibrated granular bed. *Phys Fluids*. 2003;15:3718–3729.
15. Jain N, Ottino JM, Lueptow RM. An experimental study of the flowing granular layer in a rotating tumbler. *Phys Fluids*. 2002;14:572–582.
16. Medina A, Córdova JA, Luna E, Treviño C. Velocity field measurements in granular gravity flow in a near 2-D silo. *Phys Lett A*. 1998;250:111–116.

17. Steingart DA, Evans JW. Measurements of granular flows in two-dimensional hoppers by particle image velocimetry. Part I: experimental method and results. *Chem Eng Sci*. 2005;60:1043–1051.
18. Seville JPK, Ingram A, Parker DJ. Probing processes using positrons. *Chem Eng Res Des*. 2005;83:788–793.
19. Depypere F, Pieters JG, Dewettinck K. PEPT visualisation of particle motion in a tapered fluidised bed coater. *J Food Eng*. 2009;93:324–336.
20. Chian WC, Seville JPK, Yang Z, Baeyens J. Particle motion in the CFB riser with special emphasis on PEPT-imaging of the bottom section. *Powder Technol*. 2009;196:318–325.
21. Van de Velden M, Baeyens J, Seville JPK, Fan X. The solids flow in the riser of a circulating fluidised bed (CFB) viewed by positron emission particle tracking (PEPT). *Powder Technol*. 2008;183:290–296.
22. Hoomans BPB, Kuipers JAM, Mohd Salleh MA, Stein M, Seville JPK. Experimental validation of granular dynamics simulations of gas-fluidised beds with homogenous in-flow conditions using positron emission particle tracking. *Powder Technol*. 2001;116:166–177.
23. Fan X, Parker DJ, Yang Y, K SJP, Baeyens J. The effect of bed materials on the solid/bubble motion in a fluidised bed. *Chem Eng Sci*. 2008;63:943–950.
24. Stein M, Ding YL, Seville JPK, Parker DJ. Solids motion in bubbling gas fluidised beds. *Chem Eng Sci*. 2000;55:5291–5300.
25. Laverman JA. On the Hydrodynamics in Gas Phase Polymerization Reactors. Ph.D. Thesis. Technical University Eindhoven, 2010.
26. Link JM, Deen N, Kuipers JAM, Fan X, Ingram A, Parker D, Wood J, Seville J. PEPT and discrete particle simulation study of spout-fluid bed regimes. *AIChE J*. 2008;54:1189–1202.
27. Mudde RF. Advanced Measurement Techniques for GLS Reactors. *Can J Chem Eng*. 2010;88:638–647.
28. Tapp HS, Peyton AJ, Kemsley EK, Wilson RH. Chemical engineering applications of electrical process tomography. *Sens Actuators B*. 2003;92:17–24.
29. Isaksen O. A review of reconstruction techniques for capacitances tomography. *Meas Sci Techno*. 1996;7:325–337.
30. Yang WQ, Peng L. Image reconstruction algorithms for electrical capacitance tomography. *Meas Sci Technol*. 2003;14:R1–R13.
31. Li Y, Yang W. Image reconstruction by nonlinear Landweber iteration for complicated distributions. *Meas Sci Technol*. 2008;19:094014.
32. Lei J, Liu S, Li Z, Sun M. An image reconstruction algorithm based on the extended Tikhonov regularization method for electrical capacitance tomography. *Measurement*. 2009;42:368–376.
33. Du B, Warsito W, Fan LS. ECT Studies of the choking phenomenon in a gas-solid circulating fluidized bed. *AIChE J*. 2004;50:1386–1406.
34. Liu S, Chen Q, Wang HG, Jiang F, Ismail I, Yang WQ. Electrical capacitance tomography for gas-solids flow measurement for circulating fluidized beds. *Flow Meas Instrum*. 2005;16:135–144.
35. Makkawi YT, Wright PC. Fluidization regimes in a conventional fluidized bed characterized by means of electrical capacitance tomography. *Chem Eng Sci*. 2002;57:2411–2437.
36. Du B, Warsito W, Fan LS. ECT studies of gas-solid fluidized beds of different diameters. *Ind Eng Chem Res*. 2005;44:5020–5030.
37. Godlieb W. High pressure fluidization. Ph.D. Thesis. Technical University Eindhoven, 2010.
38. Cundall PA, Strack ODL. A discrete numerical model for granular assemblies. *Géotechnique*. 1979;29:47–65.
39. Deen NG, van Sint Annaland M, van der Hoef M, Kuipers JAM. Review of discrete particle modeling of fluidized beds. *Chem Eng Sci*. 2007;62:28–44.
40. Koch DL, Hill RJ. Inertial effects in suspension and porous-media flows. *Annu Rev Fluid Mech*. 2001;33:619–647.
41. Bird RB, Steward WE, Lightfoot EN. *Transport Phenomena*. John Wiley and Sons, 1960.
42. Westerweel J. Fundamentals of digital particle image velocimetry data. *Meas Sci Technol*. 1997;8:1379–1392.
43. Van Buijtenen MS, Börner M, Deen NG, Heinrich S, Antonyuk S, Kuipers JM. An experimental study of the effect of collision properties on spout-fluidized bed dynamics. *Powder Technol*. 2011;206:139–148.
44. Link JM, Cuypers LA, Deen NG, Kuipers JAM. Flow regimes in a spout-fuid bed: a combined experimental and simulation study. *Chem Eng Sci*. 2005;60:3425–3442.
45. Link JM. Development and Validation of A Discrete Particle Model of A Spout-Fluid Bed Granulator. Ph.D. Thesis. University of Twente, 2006.

Manuscript received Dec. 17, 2010, and revision received Aug. 4, 2011.